The Astrophysical Journal Letters, 917:L18 (7pp), 2021 August 20 https://doi.org/10.3847/2041-8213/ac1866


# A Corotating Group of Dwarf Galaxies around NGC 2750 as a Centaurus A Analog

Sanjaya Paudel[1,3], Suk-Jin Yoon[1,3], and Rory Smith[2]
[1] Department of Astronomy & Center for Galaxy Evolution Research, Yonsei University, Seoul 03722, Republic Of Korea; sjyoon0691@yonsei.ac.kr
[2] Korea Astronomy and Space Science Institute, Daejeon 305-348, Republic Of Korea
*Received 2021 June 20; revised 2021 July 27; accepted 2021 July 28; published 2021 August 17*

## Abstract

We study a low-mass spiral galaxy NGC 2750 (~5 times less massive than the Milky Way), located ~40 Mpc away in a sparse region that hosts seven satellite galaxies within a projected distance of 150 Kpc. Among them six are star-forming dwarfs with stellar masses of $>\approx 10^7\,M_\odot$ and one is an early-type dwarf with a stellar mass of $2.6\times10^6\,M_\odot$. The star-forming dwarfs are gas rich, with gas mass fractions as high as $\mathrm{Log}(M_{\mathrm{H\,I}}/M_*)=1.2$ and their star formation rates vary between 0.03 and $0.35\,M_\odot\ \mathrm{yr}^{-1}$. The projected distances and measured radial velocities of the six star-forming satellites provide a high probability that they are members of the group. The radial velocity distribution of the six satellites exhibits evidence of a systematic corotation. We devise a method to quantify such a corotation signal by calculating the correlation coefficient between satellites' relative line-of-sight velocities ($\Delta V_{\mathrm{r}}$) and their sky-projected distances from the host ($R_{\mathrm{p}}$). For the NGC 2750 system, we show a clear correlation between $\Delta V_{\mathrm{r}}$ and $R_{\mathrm{p}}$, with a Pearson's R correlation coefficient $c=0.90$ and $p$-value $=0.005$. We compare the NGC 2750 system with the Centaurus A (NGC 5128) system, a previously known corotating group, and conclude that the former could be a small version of the latter but is located in an isolated field, away from the influence of the large-scale structure. The results open up opportunities to explore the galactic anisotropy phenomenon on a low-mass scale and in a rarified environment.

*Unified Astronomy Thesaurus concepts:* Dwarf galaxies (416); Galaxy groups (597); Galaxy interactions (600); Galaxy evolution (594)

## 1. Introduction

Satellite galaxies are important probes for investigating the properties of their associated central galaxies. Their number frequencies and relative positions with respect to the central hosts have been used to test our current understanding of large-scale structure formation (Bullock & Boylan-Kolchin 2017). It is well known that the Lambda cold dark-matter (ΛCDM) cosmology predicts that satellite accretion by the host galaxies should be isotropic in both position and velocity spaces. However, small-scale anisotropy is expected due to the preferential accretion of subhalos along the cosmic filaments (Libeskind et al. 2011; Shao et al. 2016). Satellites of Milky Way (MW) and Andromeda galaxies are distributed in a thin plane; in particular, the MW satellites show "corotation" of their orbits (Lynden-Bell 1976; Metz et al. 2008; Ibata et al. 2013; Pawlowski 2016). The existence of such planes of satellite galaxies around the two largest galaxies in the Local Group is difficult to explain within the ΛCDM framework (Metz et al. 2007; Gillet et al. 2015; Pawlowski et al. 2015).

A number of arguments have been put forward to reconcile these findings with the standard ΛCDM cosmology. Among them, an asymmetric host halo, filamentary accretion of satellites, and a rare exception are well discussed in the literature (e.g., Zentner et al. 2005; Libeskind et al. 2015; Shao et al. 2016; Smith et al. 2016; Hammer et al. 2018). In addition, the uniqueness of our local environment, where two massive galaxies, the MW and Andromeda, dominate the mass distribution within the 1 Mpc volume, has also been used to explain the origin of the planar satellite distribution around the both galaxies. It is suggested that a past encounter between the two induced the formation of the planar structure through the transfer of material between them (Bílek et al. 2018). The interpretations have been challenged by emerging evidence of an anisotropic satellite distribution around another massive galaxy, Centaurus A (Cen A; NGC 5128), beyond the Local Group (Müller et al. 2018). On the other hand, Ibata et al. (2014) found a correlation between the line-of-sight velocities of diametrically opposite satellite galaxies around massive hosts, and showed that such correlations are not common in the DM halos of cosmological simulations. The study, however, was restricted to the kinematic properties of diametrically opposite satellites, while ignoring the other members' contribution.

## 2. NGC 2750: A Rotating Group

### 2.1. Physical Properties of NGC 2750 and Its Satellite Galaxies

Figure 1 shows the SDSS *g-r-i* tri-color combined image of NGC 2750 and its satellite galaxies. NGC 2750 is an isolated interacting spiral galaxy (Davis & Seaquist 1983). We identify six star-forming dwarf galaxies within a sky-projected radius of 150 kpc from the center of NGC 2750[4] with a relative line-of-slight velocity ($\Delta V_r$) within $\pm300\,\mathrm{km\,s}^{-1}$. The central galaxy NGC 2750 is a nearly face-on spiral galaxy and seems tidally perturbed, with one of its arms out-flung toward the upper-right of the figure, perhaps due to a previous interaction with one of its satellites. Zaritsky et al. (2013) measured Fourier model $M=1$ distortions (lopsidedness) in the Spitzer 3.6-micron images.

For the distance to NGC 2750, NED provides a wide range of distances derived from the Tully–Fisher relation, from 8.9 to 38.9 Mpc with a median value of 17.2 Mpc (Tully & Fisher 1988; Sorce et al. 2014). The large uncertainty may be

[3] Both authors have contributed equally to this paper.

[4] A central galaxy with stellar mass of $5-10\times10^9\,M_\odot$ has a typical viral radius of 150 kpc (Sales et al. 2013).

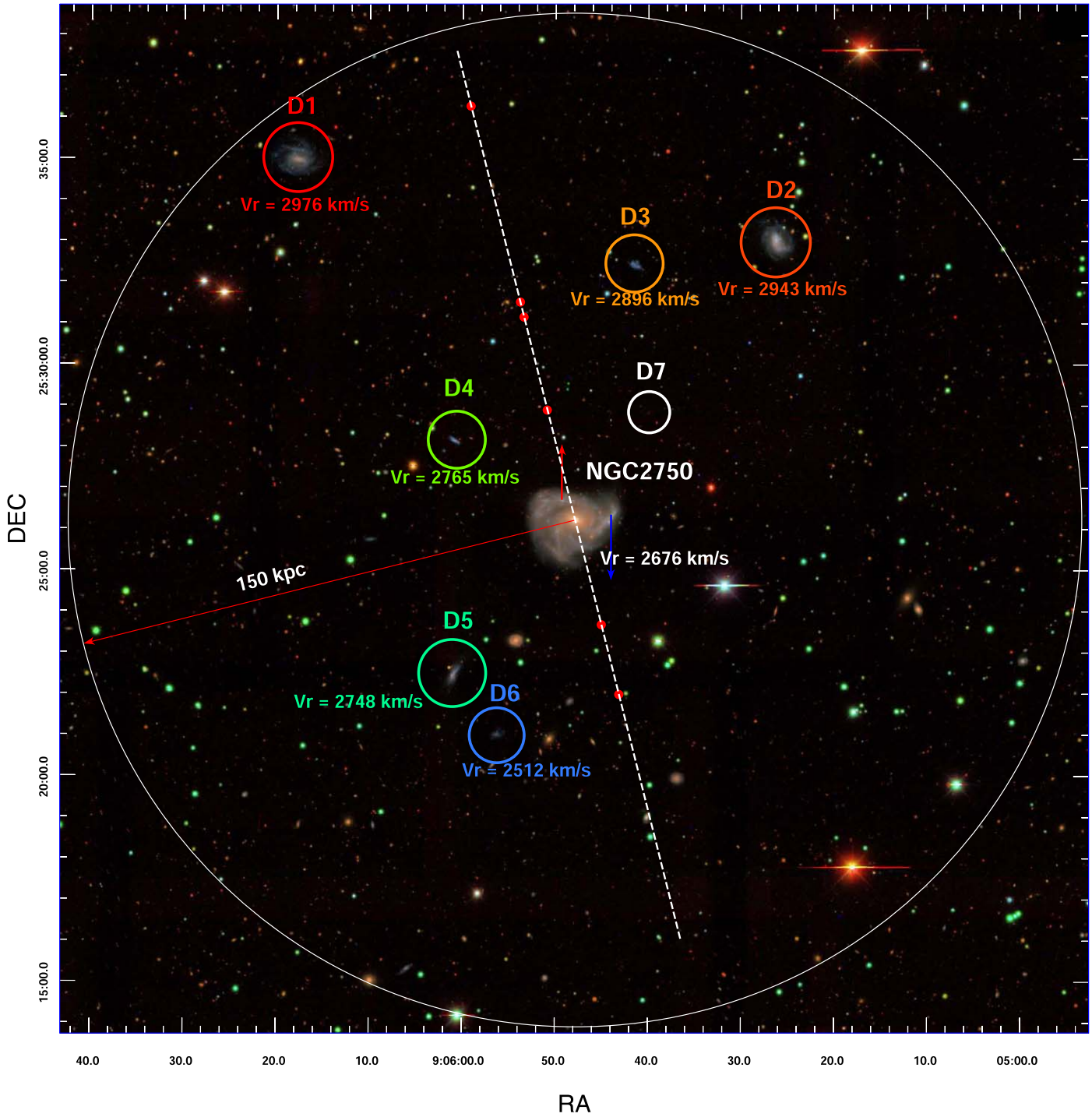


**Figure 1.** NGC 2750 and its satellite galaxies. The SDSS *g*-*r*-*i* tri-color combined image is shown with a field of view of $25' \times 25'$. The large white circle with a radius of 150 kpc encloses all satellite galaxies. Satellite galaxies are marked by small colored circles and their color represents the relative line-of-sight velocity with respect to NGC 2750. D7 is shown in white and does not have measured line-of-sight radial velocity. The observed line-of-sight velocities of the galaxies ($V_r$) are denoted next to the galaxies. The sizes of the colored circles are linearly proportional to the log of stellar masses of the satellite galaxies. The long red arrow represents the spin direction calculated as a unit vector and the white dashed lines represent the plane of rotation, perpendicular to the unit vector. The small red circle represents a projected position of satellites in the plane of rotation. We mark the two positions of NGC 2750 by the blue arrow (moving out of the page with respect to the NGC 2750 center) and the red arrow (moving into the page), for which radial velocities are measured by SDSS fiber spectroscopy.

because the galaxy is nearly face-on and disturbed, and thus an accurate calculation of the galaxy inclination is not trivial. Given the large uncertainty in the derived inclination angle, for a conservative estimate we used the Hubble flow distance for this work. We adopted a cosmology with $H_0 = 71$ and $\Omega_m = 0.3$. Thus, the derived stellar and gas masses of the galaxies in the system would be an upper limit.

We performed aperture photometry on each individual galaxy in the system using the SDSS *g*- and *r*-band images. We used similar procedures that are used in our previous work

**Table 1**
Properties of Member Galaxies in the NGC 2750 Group

| Galaxy | R.A. (deg) | Decl. (deg) | $z$ | $D$ (kpc) | $M_B$ (mag) | $g-r$ (mag) | $M_*$ ($\log(M_\odot)$) | $M_{\rm H\,I}$ ($\log(M_\odot)$) | SFR ($\log(M_\odot\ {\rm yr}^{-1})$) | 12+log(O/H) (dex) |
|---|---|---|---|---|---|---|---|---|---|---|
| (1) | (2) | (3) | (4) | (5) | (6) | (7) | (8) | (9) | (10) | (11) |
| NGC 2750 | 136.44950 | 25.43740 | 0.0089 | ⋯ | −20.31 | 0.46 | 10.04 | 9.8 | 0.12 | 8.54 |
| D1 | 136.57313 | 25.58302 | 0.0099 | 136.7 | −17.63 | 0.38 | 9.18 | 9.2 | −0.63 | 8.39 |
| D2 | 136.35975 | 25.55068 | 0.0098 | 103.5 | −18.07 | 0.29 | 9.20 | 9.3 | −0.45 | 8.23 |
| D3 | 136.42125 | 25.54005 | 0.0096 | 76.21 | −15.72 | 0.01 | 7.78 | 8.8 | −1.09 | ⋯ |
| D4 | 136.50382 | 25.46980 | 0.0092 | 45.22 | −15.53 | 0.06 | 7.79 | 8.8 | −1.16 | 8.02 |
| D5 | 136.50387 | 25.37601 | 0.0091 | 58.76 | −16.13 | 0.37 | 8.56 | 9.0 | −1.18 | 8.12 |
| D6 | 136.48540 | 25.35079 | 0.0084 | 67.21 | −14.40 | 0.16 | 7.51 | 8.7 | −1.53 | ⋯ |
| D7 | 136.41629 | 25.48070 | ⋯ | 37.72 | −11.58 | 0.78 | 6.42 | 8.7 | ⋯ | ⋯ |

**Note.** $D$ is the sky-projected separation of a satellite from the central galaxy NGC 2750. The absolute $B$-band magnitudes ($M_B$) are derived from the SDSS $g$- and $r$-band magnitudes using the color transformation equation provided by the SDSS (see the text). The optical color ($g-r$), the stellar mass ($M_*$), the H I gas mass ($M_{\rm H\,I}$), and the SFR are given in columns 7, 8, 9, and 10, respectively. In column 11, we list emission line metallicities, 12+log(O/H), derived from the $N\,II_{6548}$ and $H_\alpha$ emission line flux ratios measured in the SDSS optical spectrum.

(Paudel & Sengupta 2017) and derived the $B$-band magnitude using the equation, $m_B = g + 0.3130 \times (g-r) + 0.2271$ provided by the SDSS color conversion tool. The stellar masses were derived from $r$-band magnitudes with an appropriate mass-to-light ratio obtained from the empirical calibration provided by Zhang et al. (2017). The results are given in columns 6–8 of Table 1.

All galaxies, except D7, in this system are blue and star-forming. The $g-r$ color of NGC 2750 is 0.46 mag and those of satellites range between 0.01 to and 0.38 mag, indicating that they are blue and actively star-forming. They are also detected in the Arecibo Legacy Fast ALFA (ALFALFA) Survey (Giovanelli et al. 2005). Neutral Hydrogen (H I) emission line flux of NGC 750 measured by ALFAALFA is 22.24 Jy-km s$^{-1}$, from which we derived a total H I mass of $7.5 \times 10^9\ M_\odot$. This gives a gas mass fraction for NGC 2750 of $\log(M_{\rm H\,I}/M_*) = -0.24$. We also derived the satellites' H I content from ALFALFA flux assuming that they are located at the same distance as NGC 2750, i.e., 41.8 Mpc. They are significantly more gas rich than the host NGC 2750, with their gas to stellar mass ratios, $\log(M_{\rm H\,I}/M_*)$, varying between 0.02 and 1.2. The H I masses are given in column 9 of Table 1.

We derived the current star formation rate from the Galaxy Evolutionary Explorer (GALEX) Far-Ultra-Violet (FUV) flux using the calibration provided by Kennicutt (1998). We retrieved the GALEX all-sky survey (Martin et al. 2005) archival images from the MAST[5] server. We performed aperture photometry on the FUV-band images in the same way as we did for the SDSS images. The derived star formation rates are given in column 10 of Table 1.

The SDSS provides optical spectra of four satellites (D1, D2, D4, and D5) and the host, NGC 2750. The emission line metallicities, i.e., 12+log(O/H), are derived using a formula $12 + \log(\mathrm{O/H}) = 8.743 + 0.462 \times \frac{N\,II_{6548}}{H_\alpha}$ (Marino et al. 2013). We find that the satellites and the host have a significantly different value of 12+log(O/H), they are consistent with the mass–metallicity relation of normal star-forming galaxies, which probably indicates that they are not formed as tidal dwarf galaxies.

[5] http://archive.stsci.edu

### 2.2. Satellite Kinematics

Thanks to ALFALFA's wide-area coverage, all the star-forming satellites of the NGC 2750 system are detected in ALFALFA and have radial velocity measurements, while the SDSS spectroscopy is unavailable for two, D3 and D6. The redshifts measured by the ALFALFA and SDSS agree well with each other, within 20 km s$^{-1}$. A candidate satellite member that is early-type, D7, has no radial velocity measurement in either ALFALFA or SDSS. We therefore excluded it from further analysis of the kinematic structure of the group.

One of the important features we present in Figure 1, is the radial velocity distribution of the satellites. We mark the satellites with color circles that present relative line-of-sight velocities between NGC 2750 and the satellites. The blue and red circles represent blueshifted and redshifted satellites with respect to NGC 2750, respectively. The green circles have similar velocities to NGC 2750. Starting from below, D6, the relative line-of-sight velocity successively increases toward the north and toward D1. This gradient in the radial velocity field could be an indication of a systematic ordered motion of satellites around NGC 2750.

We cannot find any available observations that would give constraints on the two-dimensional velocity map of NGC 2750, neither in optical nor H I emission. However, we find that the SDSS spectroscopy has targeted two different spiral arms of NGC 2750. As shown in Figure 1, the upper-left spiral arm moves away from us and the right spiral arm moves toward us compared to the NGC 2750 center. It suggests that NGC 2750's disk rotation direction is consistent with its satellites' rotation direction.

In Figure 2, left panel, we show a simple phase-space diagram. The $x$-axis is the sky-projected distance of satellites from the center of NGC 2750, and the $y$-axis is the modulus of difference in the relative line-of-sight velocities between the satellites and NGC 2750. It is evident that the relative line-of-sight radial velocities increase as the group-centric distance increases, in a manner that resembles the rotation curve of a disk galaxy, i.e., the rotation curve of a system within a common DM halo (Sofue 2012).

Beyond a few Mpc, reliable and accurate relative distance measurements are inaccessible, meaning we must deal with the two-dimensional projections of galactic systems, possessing

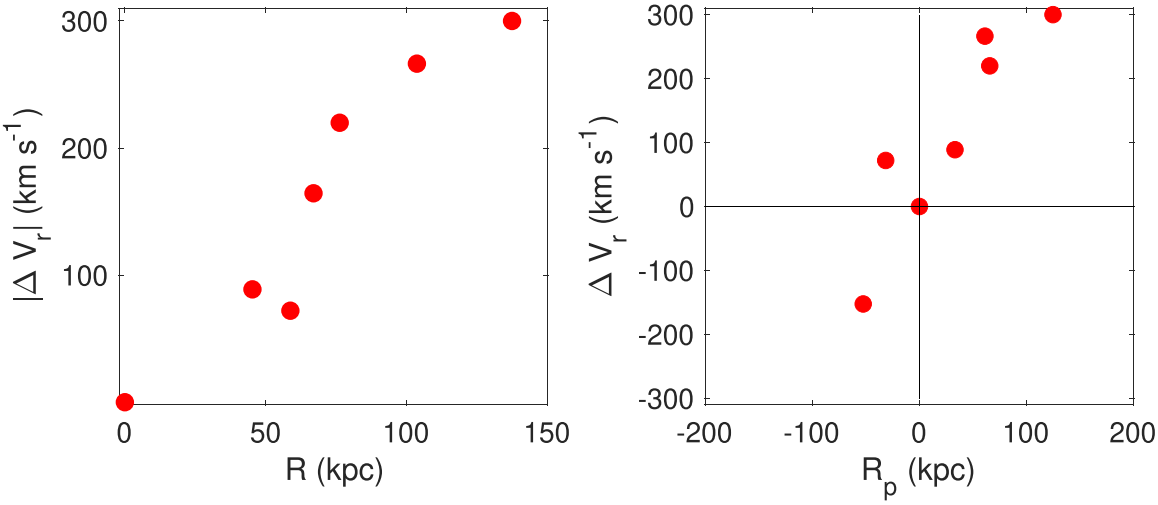


**Figure 2.** Left: a simple phase-space diagram. It is evident that the data points imitate a rotation curve of a disk galaxy. Right: relation between projected radial distances of satellites along the plane of rotation ($R_{\rm p}$) and relative line-of-sight velocities ($\Delta V_{\rm r}$). The plot shows a clear correlation between $R_{\rm p}$ and $\Delta V_{\rm r}$.

only a radial component of the velocity. In this study, we devised a method to quantify the rotation of the satellites by calculating the correlation coefficient between satellites' relative line-of-sight velocities ($\Delta V_{\rm r}$) and their projected distances from the host ($R_{\rm p}$) along the assumed plane of rotation. In general, for the flat-disk like system, e.g., CenA or Milky Way satellite system, the plane of rotation is observed along the major axis of the satellite distribution in the sky. Given the poor number distribution of NGC 2750's satellites, the calculated major axis is highly uncertain. We instead derive the plane of rotation using both kinematic and spatial information by calculating the unit vector in the sky plane, i.e, $(\hat{e_x}, \hat{e_y}, \hat{e_z}) = (\sum_{i=1}^{6} \frac{L_{x,i}}{\sqrt{L_{x,i}^2+L_{y,i}^2+L_{z,i}^2}}, ...)$, where $L = R \times V$. Since we only have two-dimensional positional (R.A. and decl.) and one-dimension velocity (line-of-sight) information, we project the z-spatial direction onto the $x$–$y$ (sky) plane and the velocities $V_{\rm x}$, $V_{\rm y}$, and $V_{\rm z}$ are projected onto the line-of-sight direction, assuming the position and velocity of NGC 2750 is an origin point. In this case $\hat{e_z}$ is always zero. As schematically shown in Figure 1, the long red arrow represents the calculated unit vector of rotation of the NGC 2750 satellites, which we assume to be the rotation axis, and the white dashed line represents the plane of rotation, perpendicular to the unit vector, which is ∼25° off from the position angle of the major axis of satellite distribution. Once we know the plane of rotation, we project all satellite positions onto the plane, i.e., small red circle in the dashed white line, and measured their linear distances from the origin, $\rm R_{\it p}$. The origin is used to assign a positive or negative sign to $\rm R_{\it p}$.

In the right panel of Figure 2, we show the relation between $\Delta V_{\rm r}$ and $R_{\rm p}$, and we calculate the correlation coefficient between them using a Pearson's R linear correlation test, which assesses the correlation between the independent variables in general. We set up a null hypothesis that the relative line-of-sight velocities between the satellites and the central are uncorrelated with their projected separation. We find a strong correlation in the case of NGC 2750, with a correlation coefficient $c = 0.90$ and $p$-value $= 0.005$, which rejects our null hypothesis with a 98% confidence level.

To assess the probability that the ordered motion of satellites could arise by chance, we performed Monte Carlo simulations. We randomize the system in three different ways,

(1) randomize relative velocities with respect to the central galaxy, NGC 2750, while keeping their positions on the sky fixed;
(2) randomize satellites' sky positions, while keeping their relative velocities with respect to the central galaxy fix; and
(3) randomize both position and velocity.

We then repeated the test one million times for each different randomization, performing the correlation test each time. We find that the occurrence of a velocity correlation similar to that in NGC 2750 in three different randomly drawn samples are ∼1.3%, ∼0.7%, and ∼0.9%, respectively.

### 2.3. Dynamical Properties

We calculated both the dynamical mass and the total projected mass of the NGC 2750 group. The dynamical mass is calculated using the maximum circular velocity 300 $\rm km\,s^{-1}$ at a radius 150 kpc. The total projected mass is calculated using the equation

$$M = \frac{32}{\pi} \frac{1}{G(N-3/2)} \sum_{i}^{N} R_{p,i} \Delta v_i^2,$$

where $\rm v_{\it i}$ and $\rm R_{\it p,i}$ are, respectively, radial velocity and projected distance of the $i$th galaxy with respect to the center of the system (Heisler et al. 1985).

The derived values of dynamical mass and total projected mass are $2.97 \times 10^{12}\,M_{\odot}$ and $3.98$[6] $\times 10^{12}\,M_{\odot}$, respectively. We calculate the total $B$-band luminosity of the system to be $2.25 \times 10^{10}\,M_{\odot}$, which gives the mass to $B$-band light ratio of 131 and 171 for the dynamical and total projected masses, respectively. These calculated mass-to-light ratios are typical of a compact group (Girardi et al. 2002).

### 2.4. Local Environment

Figure 3 shows that NGC 2750 is located in a relatively low-density environment. There is no galaxy brighter than NGC 2750 ($\rm m_{\it r} = 12.3$ mag) within a two Mpc sky-projected

[6] Considering the nearest distance of NGC 2750, i.e., 8.9 Mpc, provided by NED, the calculated value of total projected mass is $1.1 \times 10^{12}\,M_{\odot}$

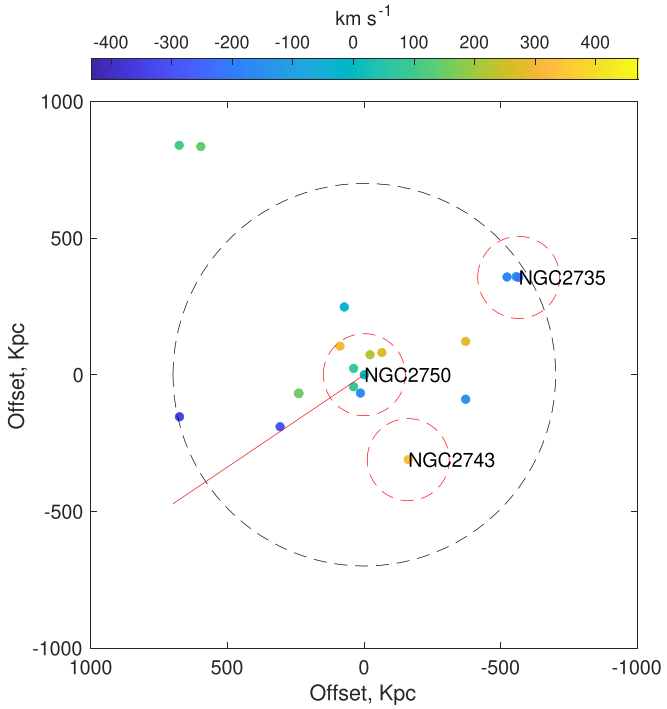


**Figure 3.** Distribution of galaxies around NGC 2750 available in NED within the velocity range of $\pm$ 700 km s$^{-1}$ with respect to the line-of-sight velocity of NGC 2750. The symbol color indicates their relative line-of-sight velocities with respect to NGC 2750, according to the color-bar at the top of the plot. The red dotted circles mark the 150 kpc sky-projected radius regions around NGC 2750, NGC 2735, and NGC 2743. The larger dotted black circle represents a 700 kpc radius centered at NGC 2750. The red line represents the axis of global rotation.

physical radius. However, we find two galaxies (NGC 2735 and NGC 2743), which are relatively bright compared to the galaxies within a 700 kpc radius centered at NGC 2750. They are located at a sky-projected distance of $\sim$700 kpc and $\sim$400 kpc, respectively, from NGC 2750. NGC 2735 is brighter than NGC 2743, but nearly two magnitudes fainter than NGC 2750 in $r$ band. NGC 2735 and NGC 2743 have relative line-of-sight velocities with respect to NGC 2750 of $-220$ km s$^{-1}$ and 350 km s$^{-1}$, respectively, which are misaligned with satellite kinematics of NGC 2750. The redshifted NGC 2743 is located at the blueshifted part of NGC 2750's satellite kinematics (i.e., toward the south), and NGC 2735 is located at the redshifted part (i.e., toward the north). This makes it unlikely that the three bright galaxies (NGC 2750, NGC 2735, and NGC 2743) and their companion satellites form a coherent large-scale structure like a filament. The redshift independent distances, cataloged in NED, show that NGC 2735 is located significantly farther than NGC 2750 at a line-of-sight distance of 51.6 Mpc from us, and NGC 2743 is located significantly nearer to us at a line-of-sight distance of 31.5 Mpc. The distance measurements suggest that these galaxies are unlikely to be gravitationally bound to each other.

Overall, there are eight additional galaxies within a 700 kpc sky-projected radius from NGC 2750. Interestingly, after removing NGC 2743, NGC 2735, and their companions (i.e., located within a 150 kpc sky-projected radius from their centers), we still find a correlation between the projected radial distances of all satellite galaxies within 700 kpc from NGC 2750 and their velocities. Repeating the correlation tests as in Section 2.2, we find a Pearson's R correlation coefficient $c = 0.92$ and $p$-value $= 0.02$. The axis of this global rotation (red line in Figure 3) is only 10° different from the rotation axis of NGC 2750's satellites shown in Figure 1.

## 3. Discussion and Conclusion

### 3.1. Cen A Analog

The Cen A system has 16 satellites within its virial radius of $\sim$700 kpc. Müller et al. (2018) statistically analyzed kinematics of the satellites around Cen A and revealed evidence of corotation of the satellites. The three-dimensional (3D) distances of the Cen A system galaxies are known and, based on this information, the plane of the satellites has been confirmed. Müller et al.'s analysis assumes the rotation of satellites along the plane of the satellites, which is nearly parallel to the major axis of Cen A. On the contrary, we do not know the 3D distances of the NGC 2750 member satellites, so it is much more difficult to verify their planar structure.

To facilitate this, we apply our analysis method to the Cen A system in projection so that we can compare the two systems more directly. The top panel of Figure 4 shows the on-sky distribution and relative line-of-sight velocities of satellites of the Cen A system. For ease of understanding, we plot differently colored filled symbols for redshifted (red color) and blueshifted (blue color) satellites with respect to the velocity of the host. The color of the large circle surrounding each filled symbol represents their $\Delta V_{\rm r}$, according to the top color-bar. Similar to NGC 2750 system in Figure 1, the two dashed lines, red and magenta, are the rotation axis and plane, respectively. The gray dots represent the projected position of satellites onto the plane of rotation.

As can be seen in the top panel, the satellite distribution around Cen A is flattened even in projection, and it shows a rotation axis that is perpendicular to the elongation like a flattened disk. In comparison, the satellite distribution around NGC 2750 does not appear strongly elongated as can be seen in Figure 1, although this may be due to poor number statistics (i.e., only six satellites).

In the bottom panel of Figure 4, we show the relation between $\Delta V_{\rm r}$ and $R_{\rm p}$ of the satellites of Cen A (blue circles). The Pearson's $R$ linear correlation test gives a coefficient $c = 0.61$ and $p$-value $= 0.008$. These values are similar to what Müller et al. (2018) found in their analysis. We also show NGC 2750 data points in red and find that the Cen A and NGC 2750 systems show a similar $\Delta V_{\rm r} - R_{\rm p}$ relationship.

### 3.2. Uniqueness of the NGC 2750 System

How unique is the NGC 2750 system? In addition to the fact that the satellites of NGC 2750 show systematic corotation, there is another important feature that is not common. NGC 2750 hosts six or more satellites with stellar masses greater than that of the Small Magellanic Cloud. However, we do not have the direct distance measurement of satellite galaxies from which we can confirm their group membership. Instead, we look at the probability that they are group members in a projected phase-space diagram (similar to Figure 2; Oman & Hudson 2016) produced with our own cosmological simulations.[7] We find that the majority have a >70% probability of being group members.

[7] A simulation of a single 120 Mpc h$^{-1}$ cosmological box conducted with Gadget-3 (Springel 2005), using cosmological parameters: $\Omega_m = 0.3$, $\Omega_\Lambda = 0.7$, $\Omega_b = 0.047$, and $h_0 = 0.684$.

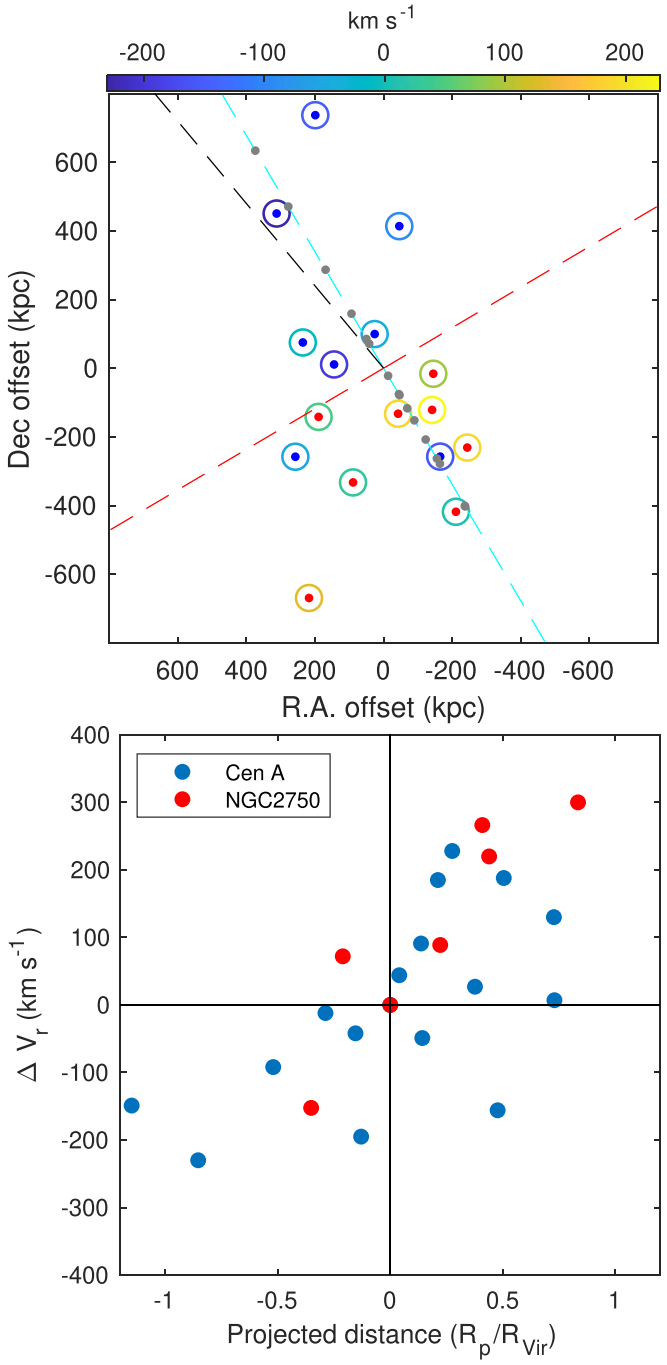


**Figure 4.** Top: the on-sky distribution of the Cen A satellite system. The approaching and receding galaxies with respect to the host are shown in blue and red, respectively. The color of the large circle represents their $\Delta V_r$, according to the color in the left color-bar. The two dashed lines, red and magenta, are the calculated axis and plane of rotation, where the gray dots represent the projected position of satellites in the plane of rotation. We also show Müller et al.'s (2018) plane of rotation with the dashed black line. Bottom: relation between $R_p$ and $\Delta V_r$ of the Cen A satellite system as in Figure 2. The Cen A data points are shown in blue and NGC 2750 data points are shown in red. The *x*-axes are normalized by the viral radius of the groups, assuming 150 kpc for NGC 2750 and 640 kpc for Cen A (van den Bergh 2000).

Observational evidence suggests that it is extremely rare to have six bright satellites with stellar masses of $M_* > 10^7 M_\odot$, even around MW-mass central galaxies. Using a systematic search for the bright satellites around the MW-mass central galaxies, the Satellites Around Galactic Analogs (SAGA) Survey found only 5 (NGC 5297, NGC 6181, NGC 6278, NGC 7166, NGC 7541, and UGC 4906) out of 36 systems that host more than five satellites with $M_* > 10^7 M_\odot$ (Mao et al. 2021). For all these systems, we performed a similar analysis of the $\Delta V_r - R_p$ co-relation for their satellites. Derived correlation coefficients for these systems are $c = 0.43$, 0.50, 0.05, 0.59, 0.66, and 0.04 and $p$-value = 0.28, 0.10, 0.87, 0.15, 0.10, and 0.92, respectively. These values show that no statistically significant correlation between $\Delta V_r$ and $R_p$ of satellites exists in these systems.

The kinematic coherence of satellite galaxies around MW, M31, and Cen A is well known. Recently, Martinez-Delgado et al. (2021) reported a spatially flattened satellite system around NGC 253 that shows a velocity correlation. In this study, we have provided additional evidence of systematic ordered motion of satellite galaxies around even low-mass host galaxy NGC 2750 with a stellar mass of $1.09 \times 10^{10} M_\odot$, nearly 5 times less massive than the MW. This may be the first such system known beyond the 10 Mpc local volume of the universe, a.k.a., the local universe. Our findings suggest that the NGC 2750 system is a small version of the Cen A system but is located in an isolated field, away from the large-scale structure. The results open up opportunities to investigate the galactic anisotropy on low-mass scale and in a rarified environment.

We thank Oliver Müller for fruitful discussions and comments on the draft version of this paper. S.P. and S.-J.Y., respectively, acknowledge support from the New Researcher Program (Shinjin grant No. 2019R1C1C1009600) and the Mid-career Researcher Program (No. 2019R1A2C3006242) through the National Research Foundation of Korea. This study is based on the archival images and spectra from the Sloan Digital Sky Survey (the full acknowledgment can be found at https://www.sdss.org/collaboration/#acknowledgements).

## ORCID iDs

Sanjaya Paudel https://orcid.org/0000-0003-2922-6866
Suk-Jin Yoon https://orcid.org/0000-0002-1842-4325
Rory Smith https://orcid.org/0000-0001-5303-6830

## References

Bílek, M., Thies, I., Kroupa, P., & Famaey, B. 2018, A&A, 614, A59
Bullock, J. S., & Boylan-Kolchin, M. 2017, ARA&A, 55, 343
Davis, L. E., & Seaquist, E. R. 1983, ApJS, 53, 269
Gillet, N., Ocvirk, P., Aubert, D., et al. 2015, ApJ, 800, 34
Giovanelli, R., Haynes, M. P., Kent, B. R., et al. 2005, AJ, 130, 2598
Girardi, M., Manzato, P., Mezzetti, M., Giuricin, G., & Limboz, F. 2002, ApJ, 569, 720
Hammer, F., Yang, Y., Arenou, F., et al. 2018, ApJ, 860, 76
Heisler, J., Tremaine, S., & Bahcall, J. N. 1985, ApJ, 298, 8
Ibata, R. A., Ibata, N. G., Lewis, G. F., et al. 2014, ApJL, 784, L6
Ibata, R. A., Lewis, G. F., Conn, A. R., et al. 2013, Natur, 493, 62
Kennicutt, R. C., Jr. 1998, ARA&A, 36, 189
Libeskind, N. I., Hoffman, Y., Tully, R. B., et al. 2015, MNRAS, 452, 1052
Libeskind, N. I., Knebe, A., Hoffman, Y., et al. 2011, MNRAS, 411, 1525
Lynden-Bell, D. 1976, MNRAS, 174, 695
Mao, Y.-Y., Geha, M., Wechsler, R. H., et al. 2021, ApJ, 907, 85
Marino, R. A., Rosales-Ortega, F. F., Sánchez, S. F., et al. 2013, A&A, 559, A114
Martin, D. C., Fanson, J., Schiminovich, D., et al. 2005, ApJL, 619, L1
Martinez-Delgado, D., Makarov, D., Javanmardi, B., et al. 2021, A&A, 652, A48
Metz, M., Kroupa, P., & Jerjen, H. 2007, MNRAS, 374, 1125

Metz, M., Kroupa, P., & Libeskind, N. I. 2008, ApJ, 680, 287
Müller, O., Pawlowski, M. S., Jerjen, H., & Lelli, F. 2018, Sci, 359, 534
Oman, K. A., & Hudson, M. J. 2016, MNRAS, 463, 3083
Paudel, S., & Sengupta, C. 2017, ApJL, 849, L28
Pawlowski, M. S. 2016, MNRAS, 456, 448
Pawlowski, M. S., Famaey, B., Merritt, D., & Kroupa, P. 2015, ApJ, 815, 19
Sales, L. V., Wang, W., White, S. D. M., & Navarro, J. F. 2013, MNRAS, 428, 573
Shao, S., Cautun, M., Frenk, C. S., et al. 2016, MNRAS, 460, 3772
Smith, R., Duc, P. A., Bournaud, F., & Yi, S. K. 2016, ApJ, 818, 11
Sofue, Y. 2012, PASJ, 64, 75
Sorce, J. G., Tully, R. B., Courtois, H. M., et al. 2014, MNRAS, 444, 527
Springel, V. 2005, MNRAS, 364, 1105
Tully, R. B., & Fisher, J. R. 1988, Catalog of Nearby Galaxies (Cambridge: Cambridge Univ. Press)
van den Bergh, S. 2000, AJ, 119, 609
Zaritsky, D., Salo, H., Laurikainen, E., et al. 2013, ApJ, 772, 135
Zentner, A. R., Kravtsov, A. V., Gnedin, O. Y., & Klypin, A. A. 2005, ApJ, 629, 219
Zhang, H.-X., Puzia, T. H., & Weisz, D. R. 2017, ApJS, 233, 13